

UNIVERSITEIT VAN AMSTERDAM

FACULTY OF SCIENCE
IOP

MSC PHYSICS
TRACK AMEP

MASTER THESIS

The creation of a potassium-40 magneto-optical trap

by

Wouter Meinster

August 2015
60 EC
September 2014 - August 2015

Supervisor:
Prof. Dr. Florian Schreck

Second supervisor:
Klaasjan van Druten

Daily Supervisor:
Dr. Benjamin Pasquiou

Contents

1 Abstract **3**

2 Introduction **4**

3 Properties of potassium **6**
3.1 Atomic structure of potassium 6
3.2 Optical properties of potassium 9

4 Potassium experiment **11**

5 Master laser **12**
5.1 Theory of an external cavity diode laser 12
5.2 Technical description of the master laser 13
5.3 Wavelength tuning 14
5.4 Characteristics of the laser 15

6 Optical setup **16**
6.1 Acousto-optic modulator 17
6.2 Tapered amplifiers 18
6.3 Optical fibres 18

7 Radio- and microwave-frequency generation **20**
7.1 Radio-frequency generation 20
7.2 Microwave frequency generation 21

8 Laser lock **22**
8.1 Doppler-free spectroscopy 22
8.2 DAVLL spectroscopy 24
8.3 Optical setup of the laser lock 25
8.4 PID controller 25
8.5 Results 27

9 Vacuum system **28**

10 Laser cooling and the MOT **30**
10.1 Laser cooling 30
10.2 Magneto-Optical Trap 30

11 2D MOT **32**
11.1 Setup 32
11.2 Performance 33
11.3 Magnets 33

12 3D MOT **35**

12.1 Setup 35
12.2 Fluorescence imaging 36
12.3 Lifetime measurements 37

13 Conclusion **39**

14 Acknowledgements **40**

1 Abstract

In this report we present the creation of a 3D magneto-optical trap (MOT) for ^{40}K. The trap is loaded from an atomic beam generated using a 2D MOT. The experiment was built by the group of Jook Walraven and used between 2004 and 2012. After that period it was largely dismantled. Only the vacuum system was left untouched the remainder of the system had to be rebuild. We have rebuild and characterised the laser system needed for both traps. For the 2D MOT the permanent magnets had to be replaced. With the refurbished experiment we achieve a loading rate from the 2D MOT into the 3D MOT of 6×10^6 atoms per second. In the 3D MOT we achieve a maximum atom number of approximately 2×10^7 atoms. The loading time and the lifetime of the 3D MOT have been measured to be 3.4 seconds and 6.4 seconds, respectively.

2 Introduction

Simulations are a powerful tool used in all fields of physics. However, simulations of many-body quantum systems on a classical computers have strong limitations. The memory a classical computer needs to encode a quantum system grows exponentially with the number of particles in the system. Consequently, a seemingly simple system of 300 spin 1/2 particles, requires more complex numbers to describe it than there exist atoms in the visible universe. And currently 30 spin 1/2 particles overwhelm the memory capacity of the largest supercomputer in existence.

Only in few special cases is it possible to approximate a quantum many-body system well enough with a classical computer to obtain precise results. Especially fermionic systems, such as many-electron systems, can often not be described by a classical computer, a property that orginates from the sign change of the many-body wavefunction under particle exchange.

Feynman already recognised this problem in the early days of computer simulation and came up with a solution. Instead of using a classical computer he proposed to build a quantum simulator. A quantum simulator is a quantum system that we can easily observe and of which we can freely tune parameters, such as the interactions. Therefore, it enables us to imitate idealized models of the complicated quantum system of interest and freely observe how it evolves.

Within the last three decades several systems that can be used for quantum simulation have been realised, such as ultracold neutral atoms and ions, superconducting circuits and quantum dots. Within this thesis we will focus on ultracold neutral atoms, which allow a large degree of control over interactions, confinement, density, temperature and other parameters. Furthermore, these systems are easily scaleable. Experiments have been done with systems ranging in particle number from a single atoms up to essentially the thermodynamical limit.

Our goal is to build such a quantum simulator with a quantum gas of neutral atoms, in our case potassium-40 (^{40}K). To achieve this we will have to cool our atoms into the nanokelvin regime, where thermal fluctuation are significantly smaller then the quantum effects we want to observe.

The experiment was built by the group of Jook Walraven to study a mixture of lithium and potassium, it was operated from 2004 till 2012. After that it was not maintained and partially dismantled. The whole potassium laser system and all the magneto-optical trap (MOT) optics were removed. Most of the individual components were still present or could easily be replaced.

To get the experiment working again we rebuild the laser system including a new master laser and all the optics near the vacuum chamber. We designed new permanent magnets for the 2D MOT and reactivated the cooling systems and the power supplies for the 3D-MOT coils.

We doubted if the vacuum quality of the experiment was still sufficient for quantum gas experiments and an important goal of this project was to determine wether the vacuum was still in a good shape. By measuring loading rate and lifetime of the MOT, we obtained a lower estimate of the vacuum limited lifetime. The estimated value is promising for the creation of a degenerate Fermi gas.

3 Properties of potassium

In order to understand the techniques used to trap potassium atoms a basic knowledge of the internal structure of potassium is needed. Therefore, we will explain at the atomic structure of potassium in section **??**. After we have a clear understanding of the internal energy structure of the potassium atom we can explain its interactions with light, which is done in section **??**.

Potassium is an alkali atoms and therefore has one electron in the outer shell, making it highly chemically reactive. Potassium has three naturally occurring isotopes. In this experiment we use two of these isotopes, namely ^{39}K and ^{40}K. The main properties of the different isotopes are summarised in Table **?? ?**.

Mass number	Neutrons	Abundance (%)	Mass (u)	Lifetime	Nuclear spin
39	20	93.25	38.963706	stable	3/2
40	21	0.012	39.963998	1.28 x 10^9 y	4
41	22	6.73	40.961826	stable	3/2

Table 1: The natural occurring isotopes of potassium and their properties **?**.

3.1 Atomic structure of potassium

In this section we will give a short introduction into the atomic physics of the potassium atom. This introduction is divided into four parts: the electronic structure, the fine structure, the hyperfine structure and the Zeeman effect.

The electronic structure of an atom originates from the Coulomb interaction between the electron and the core and is given by

$$E_n \propto -\frac{Z^2}{n^2},$$

where Z is the number of protons in the atom and n the principal quantum number. To excite an electron from one level to another requires the correct energy, which is the energy difference between the two levels **?**.

The electronic structure leads to the largest energy level separation that exists in an atom. These electronic levels are split in sub-levels creating the fine structure. The fine structure arises due to two effects. First of all the mass effect, which is caused by a relativistic correction on the mass of the electron for different angular momenta l. The energy shift caused by the mass effect is given by

$$\Delta E_{\text{mass}} = -E_n \frac{\alpha^2 Z^2}{n^2} \left(\frac{3}{4} - \frac{n}{l + 1/2} \right),$$

where α is the fine structure constant. Secondly, there is the interaction between the spin and the electronic magnetic moment, which is called the spin-orbit coupling. This is described by

$$\Delta E_{\mathrm{LS}} = \frac{\alpha^2}{nl(l+1)} E(n).$$

The total fine structure splitting is then given by

$$\Delta E_{\mathrm{fine}} = \Delta E_{\mathrm{mass}} + \Delta E_{\mathrm{LS}}.$$

The fine structure levels are split in more levels called the hyperfine structure. This splitting is caused by the interaction between the electronic magnetic moment and the nuclear magnetic moment I and is described by

$$\Delta E_{\mathrm{hf}} = \frac{\alpha_{\mathrm{hf}}}{2}(I + 1/2),$$

where α_{hf} is the hyperfine coupling constant. The value for this constant in relevant cases is given in Table **??**. Taking all these effects into account the level structure of both ^{39}K and ^{40}K is split up in multiple energy states as is shown in Figure **??**.

However, till now we have neglected any magnetic fields. In an external magnetic field the degeneracy of the different magnetic states is lifted The energy shift of a state depends on the magnetic quantum number m and is given in the low-field limit by

$$E_{hf}(B) = -\frac{\alpha_{hf}}{4} + g_I \mu_B m_f B \pm \frac{\alpha_{hf}(I+1/2)}{2}\left(1 + \frac{4m_f x}{2I+1} + x^2\right)^{1/2},$$

where, $x = \frac{(g_s - g_i)\mu_B}{\alpha_{hf}(I+1.2)} B$, μ_B is the Bohr magneton and g is the Landé g-factor, which for different cases is shown in Table **??**. For the $^2S_{1/2}$ and $^2P_{3/2}$ states of ^{40}K the energies of the different magnetic states as function of the magnetic field are shown in Figure **?? ??**.

Constant	Value ^{39}K	Value ^{40}K
α_{hf} for the $^2S_{1/2}$ state	230.859860 MHz$\times h$	-285.73 MHz$\times h$
α_{hf} for the $^2P_{3/2}$ state	6.1 MHz$\times h$	-7.6 MHz$\times h$
g_I	-0.000141935	+0.000176490

Table 2: Values for constants describing the hyperfine structure for both isotopes **?**.

Constant	Value
g_s	2.00231930436
g_J for the $^2S_{1/2}$ state	2.002294
g_J for the $^2P_{3/2}$ state	4/3

Table 3: Constants used to calculate the Zeeman effect **?**.

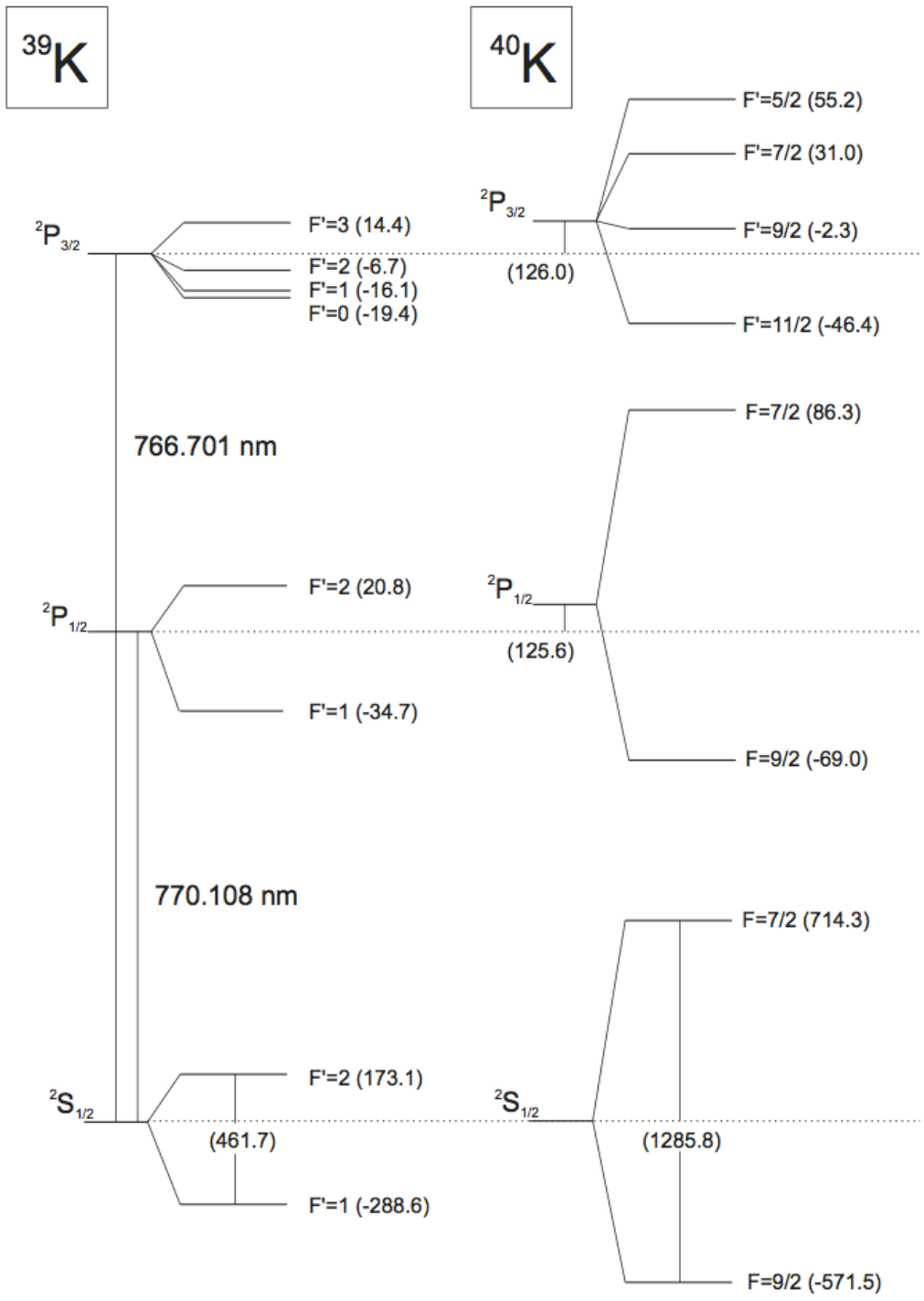


Figure 1: The level scheme of ^{39}K and ^{40}K **?**.

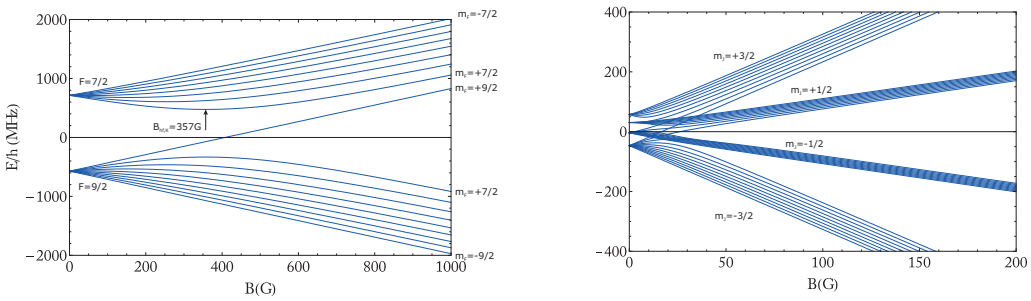


Figure 2: The energies of different m_f-states as function of magnetic field of $^2S_{1/2}$ (left) and $^2P_{3/2}$ (right) of ^{40}K **?**.

3.2 Optical properties of potassium

To understand the principles of laser cooling, a thorough understanding of the optical transitions involved is needed, which will be given in this section.

For both ^{39}K and ^{40}K we only use the transition from the ground state $^2S_{1/2}$ to the $^2P_{3/2}$ excited state manifold, also called the D2 transition. We characterize this transition by several parameters.

The first parameter is the wavelength λ of the light that drives the transition, which corresponds to a photon energy equivalent to the excitation energy. This correspondence is given by $E = \frac{\hbar c}{\lambda}$, where c is the speed of light. The wavelength can also be converted into the frequency of light $\nu = c/\lambda$ or wavenumber $k = 2\pi/\lambda$.

The second parameter is the lifetime τ of this excited state. The lifetime can be related to the natural linewidth Γ, the Full With Half Maximum (FWHM) of a transition, by the Heisenberg uncertainty principle. The Heisenberg uncertainty principle for energy and time is $\Delta E \Delta t \geq \frac{\hbar}{2}$ this uncertainty in energy can be translated into an uncertainty in frequency by using the relation between the energy of a photon and the frequency, which results in $\Gamma = \frac{1}{\tau}$

The third parameter is the recoil velocity v_{rec}. This is the change in velocity of the atom when it absorbs a photon due to conservation of momentum. The momentum conservation between the photon and atom is $P = mv_{\text{rec}} = \frac{hc}{\lambda} = \hbar k$.

Lastly, we have the saturation intensity I_s. This parameter is defined as the intensity at which the rate of photon scattering is the same as twice the decay time of the atom

$$\frac{1}{2\tau} = \frac{I\sigma}{E_{\text{photon}}},$$

where σ is the absorption cross section and E_{photon} the energy of the incoming photons. We call the intensity that satisfies this condition the saturation intensity $I_s = \frac{\pi hc}{3\lambda^3\tau}$ **?**.

If the intensity is more then the saturation intensity there will be a strong decrease in the fraction of photons absorbed from a laser beam due to the increased change of the atoms still being in the excited state.

Property	Symbol	Value
Frequency	ν	391.016170 THz
Wavelength	λ	766.7009218 nm
Wavenumber	$k/2\pi$	13042.895496 cm^{-1}
Lifetime	τ	26.4 ns
Natural linewidth	$\Gamma/2\pi$	6.04 MHz
Recoil velocity	v_{rec}	1.33573614 cm/s
Saturation intensity	I_s	1.75 $\mathrm{mW/cm}^2$

Table 4: The optical properties of ^{39}K **?**.

Property	Symbol	Value
Frequency	ν	391.0162960 THz
Wavelength	λ	766.700675 nm
Wavenumber	$k/2\pi$	13042.89970 cm^{-1}
Lifetime	τ	26.4 ns
Natural linewidth	$\Gamma/2\pi$	6.04 MHz
Recoil velocity	v_{rec}	1.30230332 cm/s
Saturation intensity	I_s	1.75 $\mathrm{W/cm}^2$

Table 5: The optical properties of ^{40}K **?**.

4 Potassium experiment

The experiment is build on two separate optical tables. The first table contains the vacuum system and the second contains the laser system. The laser system consists of four parts. Firstly, there is a potassium master laser to create a laser beam with the correct wavelength to drive the $^2S_{1/2}$, F = 9/2 to $^2P_{3/2}$, F = 11/2 transition (chapter **??**). Secondly, there is the part of the laser setup where the frequency and power of different beams is controlled by accousto-optical modulators and tapered amplifiers (chapter **??**). Thirdly, there is the generation of radio-frequency (RF) signals used to manipulate the frequency of the laser light (chapter **??**). Lastly, the master laser its frequency is stabilised by a laser lock (chapter **??**).

On the first table the vacuum system is situated (chapter **??**). Within the vacuum system we create a 2D MOT (chapter **??**) to load a 3D MOT (chapter **??**).

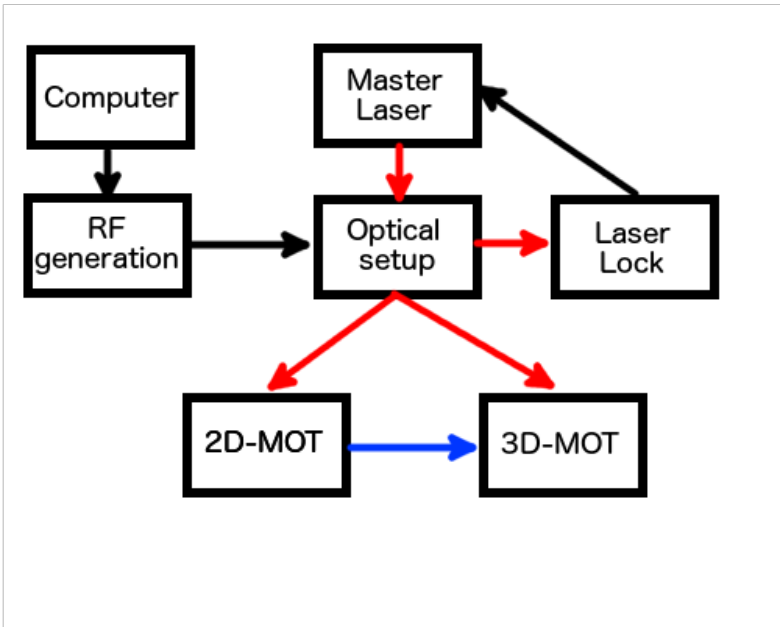


Figure 3: Schematic of the whole experiment, where the red arrows indicate laser light, black arrows indicate analog signals and the blue arrow indicates the movement of atoms.

5 Master laser

To optically cool and trap atoms we need light of a well defined wavelength. This light is generated by our master laser, which will be described in this chapter. We will give a brief introduction to the working principle of a laser (section **??**). Then we will discuss the specific details of our homebuilt master laser system (section **??**). Subsequently, the procedure to precisely tune the wavelength of the master laser system is given (section **??**). At the end of this chapter we will describe and discuss the measured characteristics of the master laser (section **??**).

5.1 Theory of an external cavity diode laser

A typical diode laser misses the capability to precisely tune the wavelength it emits and is therefore not suitable for quantum gas experiments where we have to address a single transition. To solve this problem a laser diode may be placed in an external cavity, see Figure **??**. We assume that the laser diode is anti-reflection coated and therefore we can neglect any cavity effect between the front and the back facet of the laser diode. To understand how an external cavity diode laser enables us to tune the wavelength at which the laser emits we will discuss the Littrow-configuration, as shown in Figure **??**.

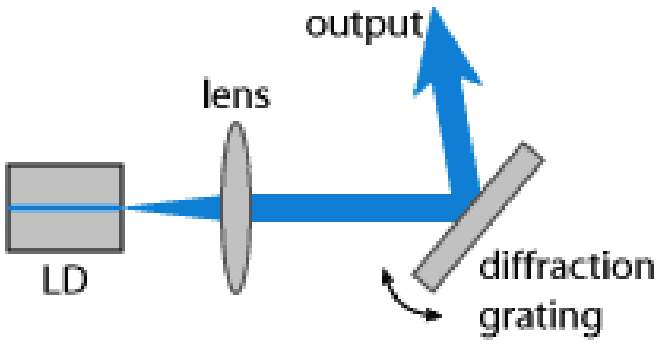


Figure 4: Schematic of the Littrow configuration **?**.

The Littrow-configuration consists of a laser diode, a collimation lens and a grating. The collimation lens is used to collimate the diverging light from the laser diode. We can use three effects to influence the wavelength at which the laser lases. The first utilises the grating to select one wavelength, as first order diffraction peak, that is reflected back into the laser diode forcing it to lase at this wavelength. By changing the angle of the grating we can change the reflected wavelength and select the wavelength at which the master laser operates. Between the grating and the back facet of the laser diode a cavity is formed. **?**.

Secondly, there is the cavity effect that allows only for certain frequency modes to exists within the external cavity. Tiny fluctuations in temperature of current can cause the laser to hop from one cavity mode into another **?**.

The third effect is the gain of the laser diode that is determined by how the diode is doped, which also depends on the temperature and current. Once the laser current is high enough and the gain overcomes the internal losses, photons will start a cascade of stimulated emission and the laser starts to emit photons of only one frequency. This state of the laser is called lasing and the minimum current at which lasing takes place is called the threshold current.

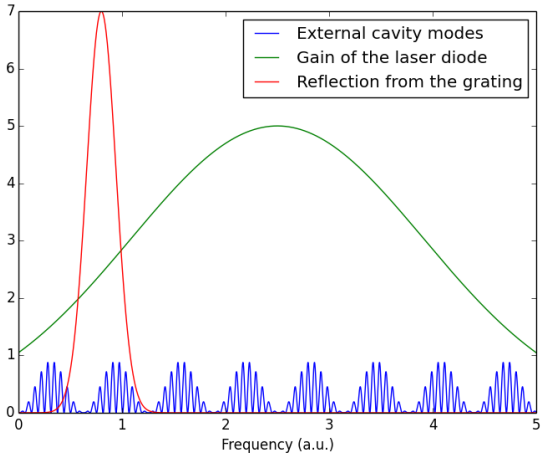


Figure 5: The combination of the different effects that determine the frequency mode in which the laser operates.

In Figure **??** all three effects are plotted. If the temperature or current changes the three lines will shift differently with respect to each other often causing the laser to hop into another lasing mode. To prevent this from happening a feedback loop is installed to compensate for any drifts, which will be discussed in chapter **??**.

5.2 Technical description of the master laser

The laser diode we use is a SAL-780-100 from Sacher Lasertechnik, which is anti-reflection coated and can be operated at a maximum current of 180 mA. The light from this laser diode is centred around 780 nm with a FWHM of 15 nm. We currently operate the laser diode at 767 nm.

To prevent electrical surges or ground loops through the optical table from influencing or damaging the laser diode the whole setup is electrically isolated from the optical table by placing a sheet of paper between the table and the laser housing. Note that paper

has an extremely low thermal conductivity, which is only twice that of air, thus the laser is also thermally isolated from the table.

The temperature is monitored using a temperature sensor chip (AD950), which is attached to the diode housing. The diode housing is thermally stabilised using a Peltier element, which is controlled by the laser controller from Sacher Lasertechnik and uses the signal from the temperature sensor to stabilise the temperature of the laser diode. The temperature of the laser diode is kept above room temperature to prevent condensation on the diode on humid days.

The wavelength at which the master laser operates is selected by the grating and is determined by the angle of the grating with respect to the laser beam. This angle can be roughly tuned by hand and precisely with a piezo element.

Due to the rectangular geometry of the laser diode the spatial mode of the laser is elliptical instead of Gaussian. We have corrected for this by placing a cylindrical lens telescope after the laser.

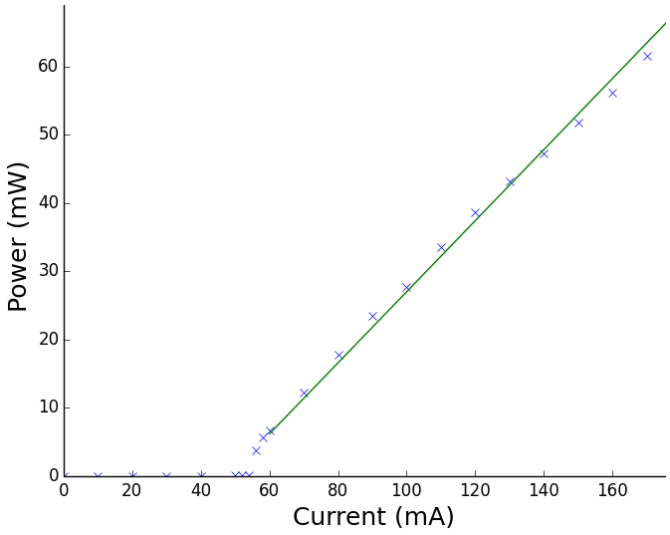


Figure 6: The relation between the input current and the output power of the laser measured after the optical isolator at a wavelength of 767 nm. The threshold behaviour is clearly visible at 55 mA.

5.3 Wavelength tuning

The wavelength is tuned in two stages. First we roughly tune it to a tenth of a nanometer then we fine-tune it to a thousands of a nanometer. During the rough tuning the wavelength is determined with the help of a wave meter. We change the angle of the grating till it is within a tenth of a nanometer from the correct wavelength, which is the accuracy of the wave meter. Then the laser output power is maximised by aligning the

back reflection from the grating on the laser diode. This process is repeated till we have a high laser output power at the correct wavelength.

During the fine tuning we determine the precise wavelength by looking at a spectroscopy signal on the oscilloscope, while scanning over a range of approximately 1 THz. The current and piezo voltage is changed till we find the characteristic signals of the ^{39}K transitions.

5.4 Characteristics of the laser

We characterised the relation between current and output power at 767 nm, which is shown in Figure **??**. The threshold current and the total output intensity is significantly lower than the characteristics from the datasheet, which is shown in Figure **??**. However, the data from the datasheet is taken at 780 nm whereas we operate the laser at 767 nm. As the gain of the laser diode is significantly lower at this wavelength our higher threshold current is expected. Furthermore, we checked if the laser is operating singlemode by identifying the frequency mode(s) with the help of a Fabry-Pérot cavity.

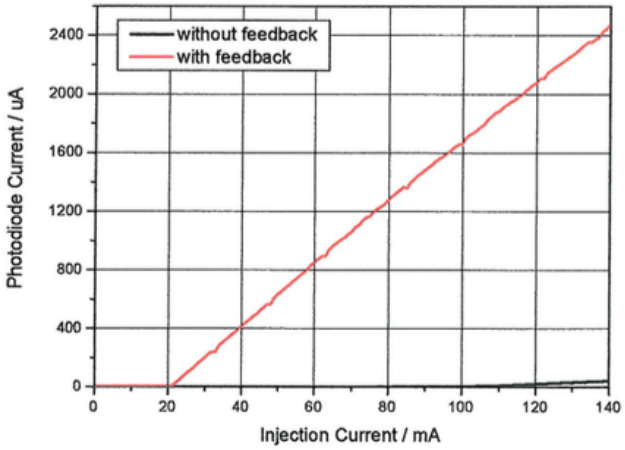


Figure 7: The relation between the diode laser current and the power of the laser from the datasheet. This data was taken at a wavelength of 780 nm. The threshold behaviour is clearly visible at 20 mA.

6 Optical setup

The master laser produces coherent light but only at one frequency with a relative weak power of 60 mW. To conduct our experiments we want to have individual control over both the frequency and the power of several beams. Control over the laser beams is achieved by utilising acousto-optic modulators (section **??**). The power of the master laser is not sufficient to trap enough atoms for our experiment, therefore the laser light is amplified by tapered amplifiers (section **??**). Laser light at the desired power and frequency is then guided to the main experiment by optical fibres (section **??**). The full optical setup is shown in Figure **??**.

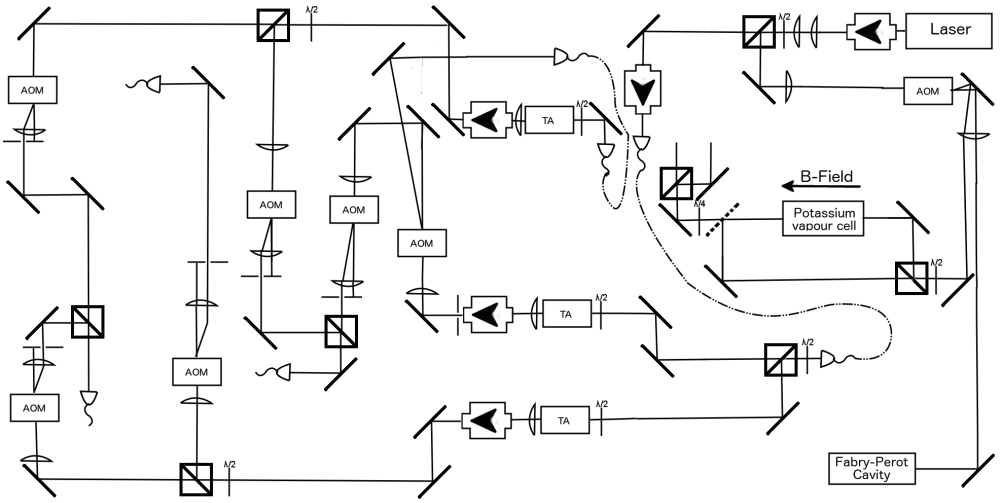


Figure 8: Schematic of the optical setup.

The setup is used to prepare three different laser beams. Firstly, there is the laser beam that is used for the 2D MOT. Secondly, there is the laser beam that is used for the 3D MOT. Lastly, there is the laser beam that used to push the atoms from the 2D MOT into the 3D MOT, which we call the push beam. The functions of these beams are explained in chapters **??** and **??**.

Both the 2D-MOT beam and the 3D-MOT beam consist of light with two different frequency components. One frequency component is red detuned from the $^2S_{1/2}$, F = 9/2 to $^2P_{3/2}$, F = 11/2 transition. As this light is used to trap the atoms we will call this the trap light. The other frequency component is slightly red detuned from the $^2S_{1/2}$, F = 7/2 to $^2P_{3/2}$, F = 9/2 transition and is called the repump light. In contrast to other elements such as rubidium the power of the repump light required for K^{40} is not negligible compared to the trap light. Therefore, the force of the repump light on trapped atoms is significant and it has to be mixed into the trap light. To balance the light pressure of the repump light, we mix that light into all beams used for laser cooling. An overview of the frequencies used in the experiment can be found in Figure **??**.

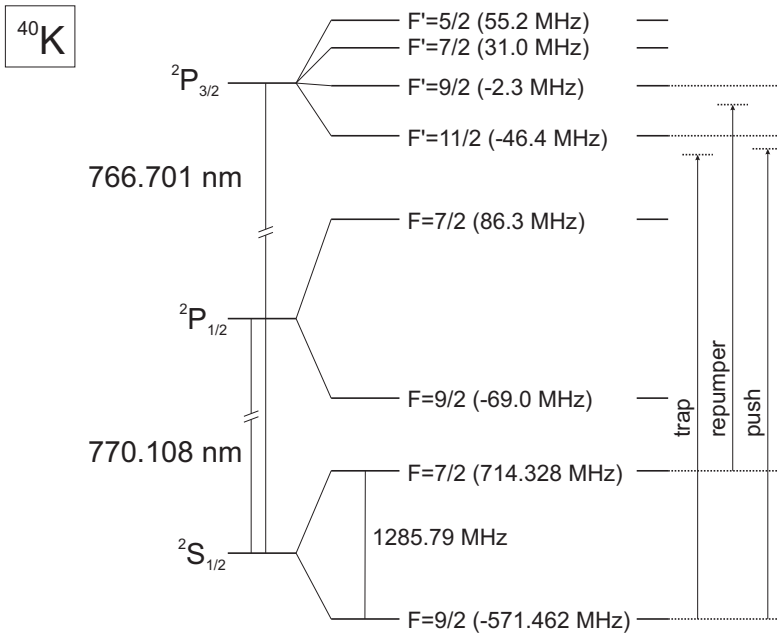


Figure 9: Schematic of the frequencies used in the experiment **?**.

6.1 Acousto-optic modulator

To control the frequency, with sub-megahertz precision, and the power of the laser light we use acousto-optic modulators (AOMs). As shown in Figure **??** the AOM consists of a piezo element attached to a crystal. By sending an RF-signal into the piezo, an acoustical wave is created in the crystal, which can be seen as a density grating. Light that propagates at the Bragg angle with respect to that grating can reflected into the first order. The law of conservation of momentum requires this light to either absorb or emit a RF-phonon changing the frequency of the laser light by one quanta of the RF-signal, thereby allowing us to change the laser frequency with sub-Hz level precision.

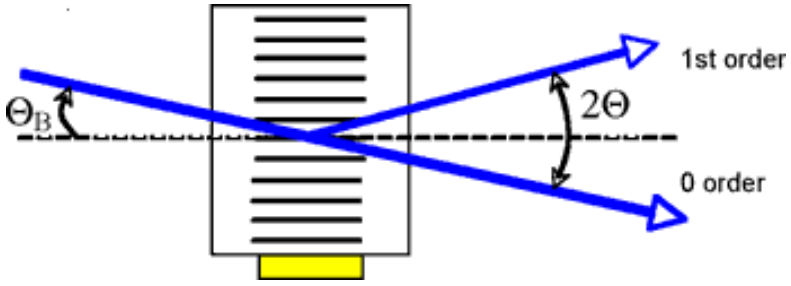


Figure 10: Schemetic with the working principle of an AOM.

Most AOMs we use are ISOMET-1205 AOMs, which have a central frequency of 80 MHz

and a bandwidth of 30 MHz. We have two other AOMs in our setup. The first is the AOM used for spectroscopy, which operates at 265.2 MHz. There were no AOMs available that work at this frequency, therefore we took a Gooch and Housego 3200-124 AOM, which originally has a centre frequency of 200 MHz and a bandwidth of 50 MHz. We changed the coil of the LC circuit inside the AOM in such a way that it efficiently absorbs RF signals at 265 MHz. The downside of this procedure is that the impedance matching now only works in a very small range of frequencies, therefore this AOM can now only be used efficiently at 265 MHz.

To overcome the large frequency gap between the F=7/2 and F=9/2 state of ^{40}K, which is needed for the repump light, we use an AOM that changes the frequency by 1.2085 GHz. This is a custom made AOM from Brimrose (GPF-1240-200-.766), the Brimrose AOM.

6.2 Tapered amplifiers

The master laser does not provide sufficient power to trap enough potassium atoms for quantum gas experiments. Therefore, we use three tapered amplifiers (TAs) to amplify the laser light. All TAs contain the same chip from EagleYard (EYP-TPA-0765-01500-3006-CMT03-0000). The spatial mode coming out of the TA is rectangular due to the chip geometry. By using a cylindrical lens to deform the rectangular mode to a square we increase the coupling efficiency into the fibres. However, the overlap with the Gaussian mode of the fibre is still not perfect, therefore the maximum coupling efficiency into the fibres after the TAs is only fifty percent.

The TA is injected with a seed, light at the correct frequency, which is amplified by the TA by stimulated emission. The output power of a TA is very sensitive to the position where the laser light hits the chip. To reduce spatial movement of the TA chip it is mounted in a homemade housing that is extremely stable. By using a smart geometry thermal expansion in this housing is translated into a rotation of the chip rather than a displacement, which increases the pointing stability of the TA **?**.

The TAs are temperature controlled with Thorlabs temperature controllers. They are kept above room temperature to prevent condensation on humid days. However, while two TAs are able to stabilise the temperature without any help, the third TA requires additional water cooling to keep the temperature stable. The reason for this behaviour is unknown as this is the same chip in the same housing as the other two TAs and is operated at a lower current.

6.3 Optical fibres

The optical fibres are either from Schäfter+Kirchhoff or from Thorlabs. Both types are polarisation maintaining and designed for a wavelength of 780 nm. All fibres have been

cleaned and the fibres that showed burn marks have been repolished. To ensure the optical fibres are polarisation maintaining we have aligned the polarisation axis of the fibres with the direction of polarisation of the linearly polarised laser light with the help of the polarimeter.

7 Radio- and microwave-frequency generation

To shift the frequency of laser light we often use AOMs. As mentioned in the previous chapter the AOMs need to be driven by an RF signal. The scheme used to generate the RF signals is shown in Figure **??**. This RF signal is created at the desired frequency by a voltage controlled oscillators (VCO). The power of a signal is than decreased by a voltage controlled attenuator (VCA). To function efficiently the AOMs need more RF power then the VCO can produce, therefore the signal is amplified by an amplifier.

We will discuss the components we use to create the RF signals and briefly describe how we control those components (**??**). The frequency required for the Brimrose AOM is generated in a different way than the other RF signals(section **??**).

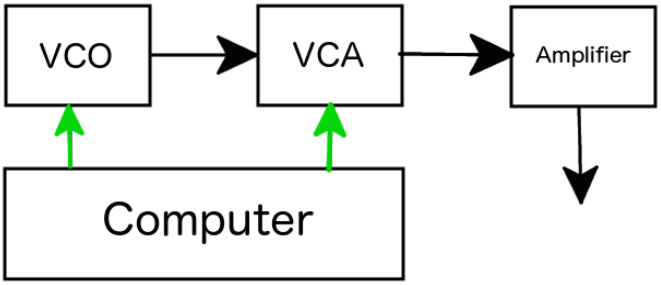


Figure 11: Schematic showing the creation of RF signals driving the AOMs.

7.1 Radio-frequency generation

The radio-frequencies (RF) are generated by VCOs. The VCOs create a radio-frequency that can be controlled by changing the voltage applied to the control port. We currently use three different sorts of VCOs. The ZOS-100, ZOS-150 and the ZOS-300 all from mini-circuits. The ZOS-100 can be tuned from 50 to 100 MHz, the ZOS-150 from 75 to 150 MHz and the ZOS-300 from 150 to 280 MHz. The RF output power of all three VCOs is 9 dBm.

After every VCO a VCA is placed. The VCA allows us to precisely control the power of the RF signal by changing the control voltage applied to the VCA. We use a ZX73-2500 from mini-circuits as VCA, which can attenuate the RF power between 3 and 55 dB.

After the VCA the signal is amplified again to obtain the power levels required to drive the AOMs. This amplification is done by a ZHL-2 or a ZHL-3(a) amplifier from mini-circuits. They add respectively 16 and 24 decibels to the incoming signal with a maximum output of 29 dBm. Note that amplifiers can easily be damaged by injecting a signal into the output port. This already occurs when nothing is connected to the

output port. Because of this situation the output signal will be reflected back into the amplifier.

The combination of the ZOS-300 with the amplifier is due to unknown reasons not able to provide the 29 dBm that is required to drive the AOM. Therefore, we added a pre-amplifier, which adds another 15 dB, between the VCA and the amplifier. The pre-amplifier used is a ZFL-500LN from mini-circuits.

The VCOs and VCAs are controlled by changing the control voltage that they receive. To control the individual devices we use a control system developed by Todd Meyrath and Florian Schreck. The control system allows us to control analog ports with a program. More information regarding the control system or software is available in **?**.[1]

7.2 Microwave frequency generation

The repump light has to be shifted by 1.2 GHz to overcome the hyperfine splitting of ^{40}K, which falls outside the frequency range that we can achieve with the available VCOs. Therefore, we used an external signal generator, the SMB100 from Rhode & Schwarz, which has a range from 7 kHz till 3.2 GHz. This signal generator gives us precise control over both the frequency and power that is supplied to the Brimrose AOM. However, this device is quite expensive and an overkill for this task, therefore we suggest to replace it in the future by a cheaper alternative. We currently pursue the design of a homemade VCO-DDS board based on a frequency doubled Analog Devices ADF4351, which could produce this frequency.

[1] The analog output ports of the system give a voltage between -10 and 10 V. However, the ZOS-100 VCO produces only 80 MHz at 10 V and we would like to be able to operate the AOMs above 80 MHz. Therefore, we changed all the ports of card B of the system to give a maximum of 13 V. This increase has been achieved by adding a 330 Ohm resistor between connection R58-R65 and the ground. The whole schematic of the board can be found in the appendix. Note that this change has not been implemented in the control software, consequently 10 V in the control software on one of the B ports is equivalent to 13 V.

8 Laser lock

In chapter **??** we discussed the huge sensitivity of the master laser to external effects. To ensure that the laser does not drift away from the desired frequency over time we created a feedback loop that will compensate any drifts. This feedback loop is called the laser lock and will be discussed in this chapter. The signal the laser lock uses to correct the laser is created by Doppler-free DAVLL spectroscopy. Therefore, a quick introduction in Doppler-free spectroscopy will be given (section **??**). Which we than expand to Doppler-free DAVLL spectroscopy (section **??**). Than the setup for the spectroscopy is described (section **??**). Subsequently, we discuss the PID controller which creates the error signal (section **??**) and lastly the performance of the lock (section **??**).

8.1 Doppler-free spectroscopy

Spectroscopy is a major analysis tool in science. The technique is used to determine the energies of excited states by measuring the absorption of light by the sample in dependence of wavelength.

One of the challenges in spectroscopy of narrow lines such as the atomic transition in potassium is Doppler broadening. Doppler broadening arises because a gas has a velocity distribution following the Maxwell-Boltzmann distribution

$$f(v) = \left(\frac{m}{2\pi kT}\right)^{3/2} 4\pi v^2 \exp\left(-\frac{mv^2}{2kT}\right).$$

Atoms with a velocity component parallel to the propagation direction of the laser will experience the frequency of the laser Doppler shifted to

$$\nu' = \nu + \frac{2\pi v}{\lambda}.$$

Atoms with different velocities absorb light with different frequency, thereby broadening the spectroscopy signal. For a gas at room temperature the Doppler broadening is in the range of several hundred megahertz. Because the spectral line we want to resolve has a width of at most several megahertz we need a trick to circumvent the Doppler broadening, called Doppler-free spectroscopy

The Doppler-free spectroscopy setup, as shown in Figure **??**, uses two beams: the pump beam (1) and the probe beam (2). The pump beam is a high intensity beam used to excite all the atoms. The probe beam is the beam used to measure the signal. If the atoms are moving they will experience opposite Doppler shifts on both beams. The pump beam will excite only atoms that are not resonant with the probe beam and the probe beam will still be absorbed. However, if the velocity of the atom is zero the pump and probe beam will both excite the atom. The excitation of zero velocity atoms by the pump beam will make the gas more transparent for the probe beam **?**.

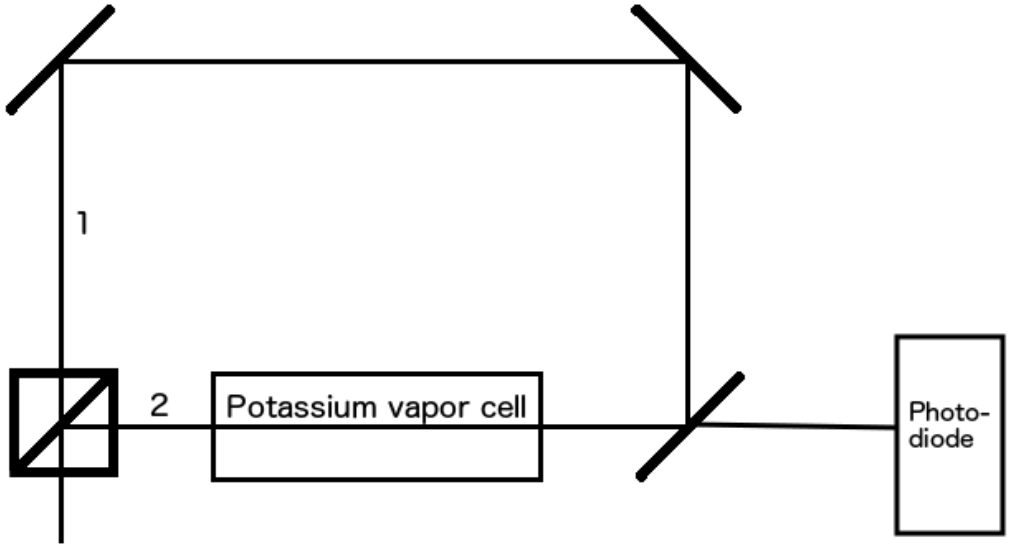


Figure 12: The setup used to for Doppler-free spectroscopy.

If the ground state has a hyperfine doublet, as is the case for potassium, a third signal will appear exactly between the spectroscopy signals corresponding to the hyperfine states. This third spectroscopy feature is called the cross-over signal and is created at the laser frequency for which the Doppler shift causes one hyperfine ground state of the atom to be on resonance with the probe and with the other state with the pump beam.

There is a small effect that will still broaden the Doppler-free spectroscopy signal. The pump beam will also excite atoms further from resonance and they can decay into a dark state. As the lifetime of this state is significantly longer then the time an atom needs to pass the beams, it will not be affected by the probe beam and thereby enhance the transmission. This effect will cause the linewidth of the signal to be larger than the linewidth of the transition depending on intensity and coupling rates from the dark state **?**.

In our experiment we have chosen to do spectroscopy on the ^{39}K isotope because it is has a high abundance and therefore is easier to detect then the low abundance isotopes. We have done Doppler-free spectroscopy on ^{39}K to find the optical transition at which we want to lock the laser. We scanned a large interval of frequencies by adding a sawtooth ramp to the piezo voltage. The sawtooth ramp is created by a frequency generator operating at 200 Hz.

This results in the spectrum that is shown in Figure **??**. This spectrum is taken at zero magnetic field. In the inset the gaussian absorption feature of the Doppler broadening

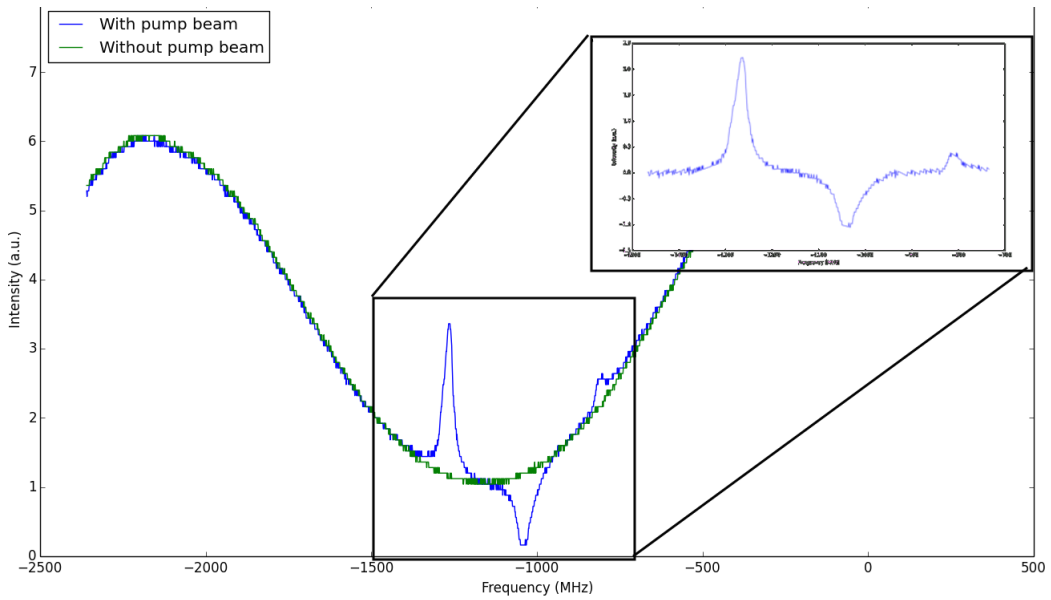


Figure 13: Spectroscopy on ^{39}K with a zoom in on the transition from the $^2S_{1/2}$ F = 1 and F = 2 states to the unresolved $^2P_{3/2}$ states with a subtracted background.

has been subtracted so we could precisely fit the location of the transition from $^2S_{1/2}$, F=1 and F=2 state to the unresolved $^2P_{3/2}$ manifold. Using to known hyperfine splitting of these states, we calibrated the frequency axis of this plot **?**.

8.2 DAVLL spectroscopy

This spectrum allows us to determine at which frequency the laser is operating. However, the spectroscopy signal is not suitable to lock a laser due to the symmetry around the desired lock point. This symmetry makes it hard to distinguish wether the laser is drifting towards lower or higher frequencies. The signal we want to lock on should be anti-symmetric around the optical transition. To achieve this we adapted the setup to perform DAVLL spectroscopy.

The DAVLL technique utilises the Zeeman effect, which increases the splitting of the magnetic levels in the excited state by applying a magnetic field. For simplicity we assume the case that the ground state does not experience a Zeeman shift. Both the pump and the probe beam are linearly polarised, which can also be described as a superposition of both σ^+ and σ^- polarised light. An optical transition will either absorb σ^+ or σ^- polarised light, thereby leaving the remaining probe light elliptically polarised. By using a quarter wave plate (QWP) and a polarisation beam splitting cube (PBC) we can split the probe light into the σ^+ and σ^- polarisation components. If we then subtract these two signals a dispersive error signal is obtained as is shown in Figure **?? ?**.

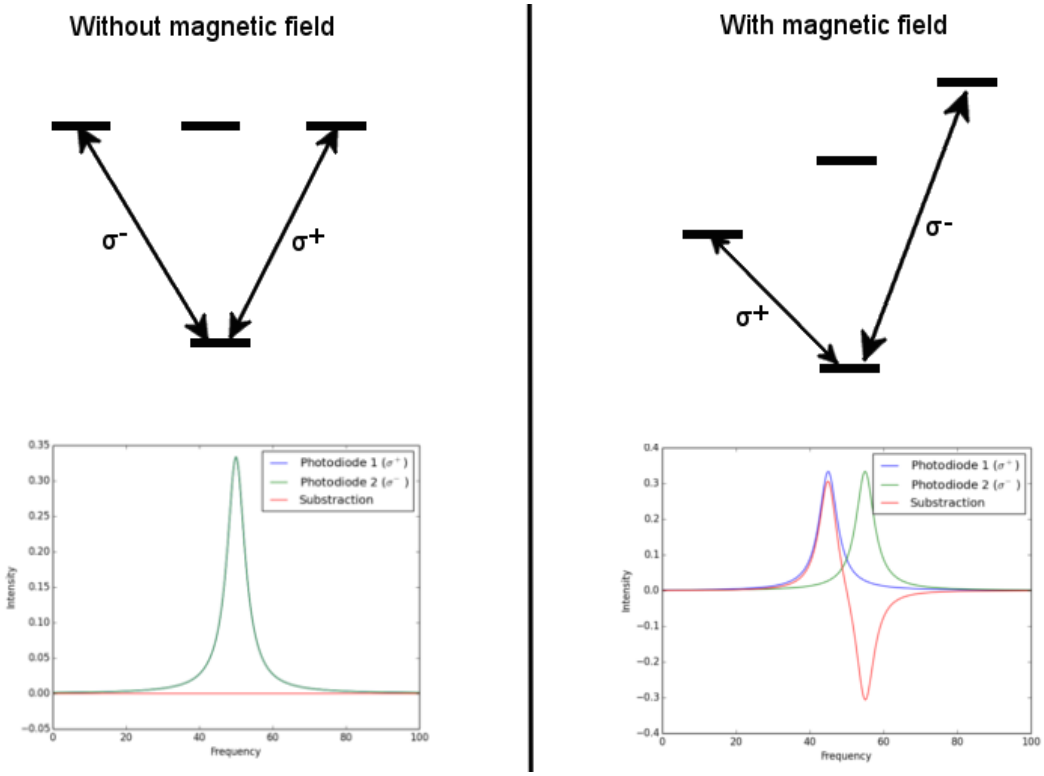


Figure 14: The principle of the DAVLL technique.

8.3 Optical setup of the laser lock

To stabilise the laser at the desired frequency we built a laser lock that utilises DAVLL spectroscopy to create an error signal. spectroscopy setup for the lock and the adaption of electronics to create the error signal has been done by Maarten Mooij. A more extensive description of the laser lock can be found in this bachelors thesis **?**.

Our master laser provides us with two different ways to correct for a drifting wavelength. One way is by changing the piezo voltage, which can correct with a bandwidth of 2.5 KHz and is called the slow correction. The other way of correcting is to change the laser current, which enables us to apply corrections with a bandwidth of 10 KHz and is called the fast correction **?**.

8.4 PID controller

The signal for both the slow and the fast corrections is created by a proportional-integral-derivative controller (PID). The correction signal is the sum of three contributions. First the proportional part determines at how big the error is at a given moment and provides a contribution to the correction signal proportional to that error. The integrator part

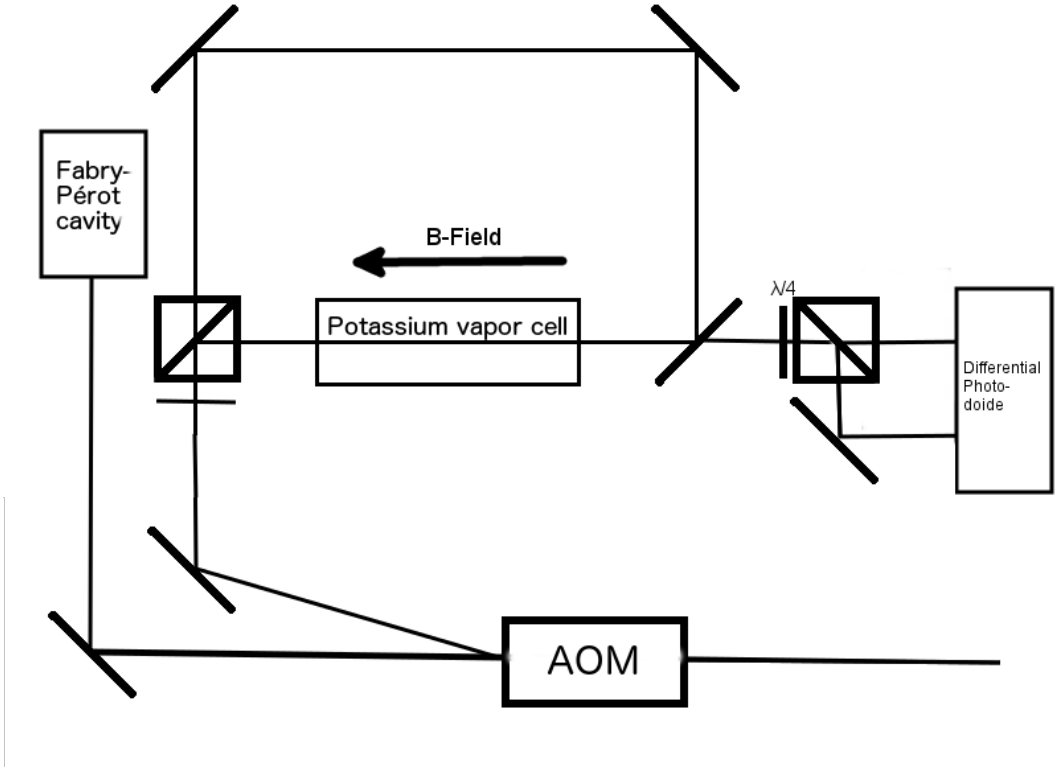


Figure 15: The setup used to generate the error signal to lock the laser.

makes corrections based on the effect that it had in the past and the differentiation part predicts how the signal will change and takes this into account for the correction. This enables the PID to stabilise in a more precise way than providing only a proportional error signal. The two most important properties that we can tune within the PID to improve its performance are the overall gain and the integration time of the integrator. Where the gain determines how strongly it compensates a change. When the gain is too low a change in frequency will not be fully corrected by the lock. By contrast, if the gain is to high it will overcorrect and the system will start to oscillate.

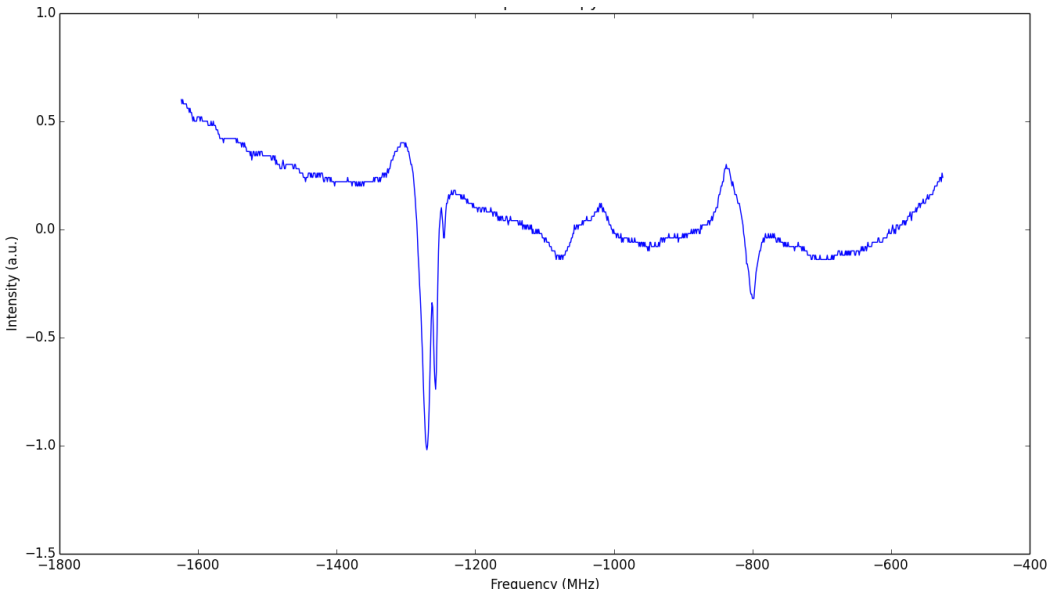


Figure 16: Signal of the DAVLL spectroscopy. The $^2S_{1/2}$, F = 1 to $^2P_{3/2}$ transition results in a nice dispersive signal.

8.5 Results

To determine the quality of the lock the most important feature of the error signal is its slope. From the spectrum shown in Figure **??** we determined that the slope of the error signal is 63 MHz/V. We also investigated the long term stability by recording the vertical drift at intervals of more than one hour. The standard deviation of these measurements is 55 mV, which corresponds to 3.5 MHz. The total range that was observed over three days is 160 mV, which corresponds to 10 MHz. From these measurements we can conclude that the lock will stay within the linewidth of the transition, which is 6 MHz, during a day. The noise on the signal itself is 15 mV corresponding to a signal to noise ratio of 40 and a laser frequency noise of 0.9 MHz.

A more thorough study of the laser lock and responses to external noise has been conducted by Maarten Mooij and can be found in **?**.

9 Vacuum system

The vacuum system, as shown in Figure **??**, consists of three connected chambers: the potassium chamber (A), the main chamber (B) and the lithium chamber (C). During the experiments we used the potassium chamber and the main chamber, which will be discussed in the coming chapter. There is a valve that can be used to disconnect the lithium chamber from the main chamber, however, closing this valve disconnects one ion pump from the main chamber, consequently we decided not to close it.

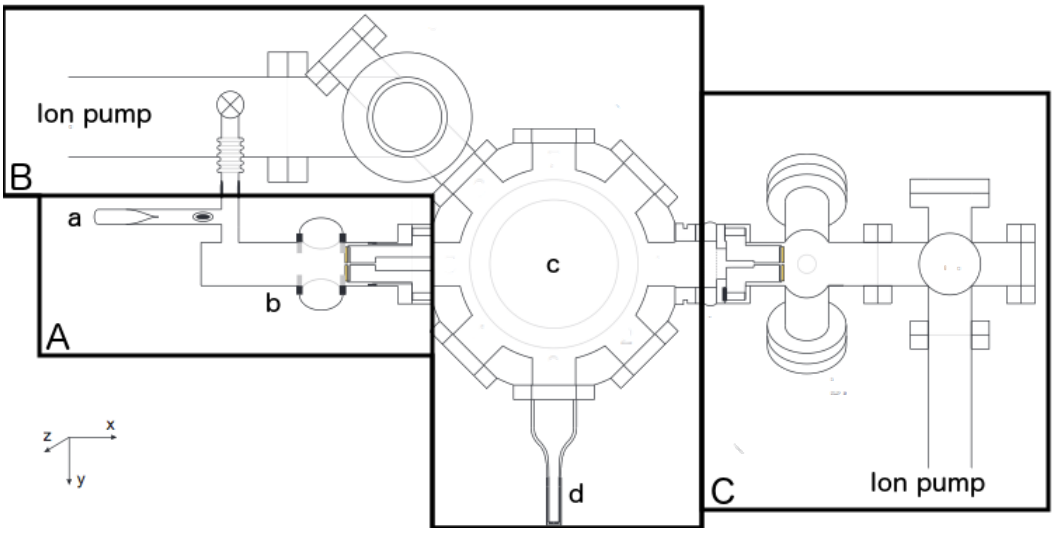


Figure 17: The schematic of the vacuum system **?**.

The potassium chamber consists of a glass ampule (a), wherein the potassium is stored. The potassium that we use is enriched to six percent of ^{40}K. The ampule is connected through a glass T-piece to the 2D-MOT chamber (b). The 2D-MOT chamber has five optical grade windows of which four are used for the 2D-MOT beams, the other one is used for the push beam but can also be used to add an optical molasses beam or probe beam. Because earlier work done on potassium experiments mentions adsorption of potassium on stainless steel all the components for the potassium chamber are made of glass.

The 2D-MOT chamber is connected to the 3D-MOT chamber (c) by a differential pumping tube with a diameter of 2 mm and a length of 23 mm. The differential pumping tube is used to separate the low quality vacuum of the 2D-MOT chamber with the ultrahigh vacuum of the 3D-MOT chamber. A gold coated mirror with a 2 mm hole is placed in front of the differential pumping tube. The mirror can be used to reflect back an optical molasses beam or probe beam for the 2D MOT.

The main chamber has seven optical grade windows of which six are used for the 3D-MOT beams. The seventh was formally used to transport the MOT to the science

chamber (d). The science chamber has been added to have both good optical access to the atomic cloud and the possibility to install strong electromagnets around the chamber for experiments. However, as we do not use this feature of the system we now use this window to image the MOT **??**.

The potassium ampule and the 2D-MOT chamber are thermally isolated with aluminium foil and can be heated to fifty degree celsius by using heating bands to increases the vapour pressure of potassium to a sufficient level. The heating bands are powered by several different power supplies. The temperature of the vacuum system is monitored by several K-type thermocouples that can measure temperatures up to 1250°C with an error of 0.4%. The thermocouples are read out by homemade electronics in order to display the values on a computer screen.

10 Laser cooling and the MOT

To achieve a Fermi degenerate gas the atoms have to be cooled to the nanokelvin regime. The first step to achieve this is to trap the atoms in a MOT. In this chapter we will first discuss the principle of laser cooling (section **??**) and then expand this to describe the behaviour of atoms in a MOT (section **??**).

10.1 Laser cooling

To understand laser cooling we will first consider the one dimensional case. The atoms are cooled by two counter-propagating beams with a frequency that is red detuned from the laser cooling transition. Since, the beams are red detuned, the Doppler effect causes an atom that moves against one beam to be closer to resonance and more detuned from the other beam. Therefore, the atom will absorb more photons from the beam it moves against. When the atom absorbs a photon from this beam the photon will transfer its momentum to the atom. The excited atom will after some time emit a photon in a random direction, again changing its momentum. The momentum change the atom undergoes in the emission process will be averaged out over many absorption-emission cycles, resulting in a friction force that slows the atoms down. This process is called optical molasses **?**.

10.2 Magneto-Optical Trap

Optical molasses reduces the temperature of the atomic gas. To reach high phase-space density, we also want to increase the density of the gas by collecting the atoms in a small volume, thereby forming a cold and dense cloud. To trap the atoms in this volume, we modify the optical molasses scheme and create a MOT. Just like optical molasses the MOT works with two counter propagating beams. But we now make the force the laser beams exerts on the atom not only velocity dependent but also space dependent. This will result in a force pushing the atoms into a small volume.

We assume an atomic system with a $J = 0$ ground state with F = 0, which is unaffected by the magnetic field. For the excited state we assume $J^{'} = 1$ which in the presence of a magnetic field it will split up in three different magnetic states. The $m_J = 1$ can only be reached from the ground state by σ^+ polarised light and $m_f = -1$ only by σ^-.

In Figure **??** the magnetic states are shown in the presence of a magnetic field, which is oriented along the direction of propagation of the laser beams. The magnetic field has a gradient, which is also oriented along this axis and which results in zero magnetic field in the centre of the MOT. By choosing σ^+ for one beam and σ^- for the other the atoms in presence of a magnetic field will be resonant with only one of the two beams. By construction, an atom to the left of the magnetic field zero will absorb more photons from the beam coming from the left and therefore be pushed towards the centre, If the

atom is to the right of the magnetic field zero, more photons are scattered from the beam coming from the right, also pushing the atom to the centre. Near the zero magnetic field the Zeeman splitting can be neglected and optical molasses as described in the previous section will cool the atoms down **?**.

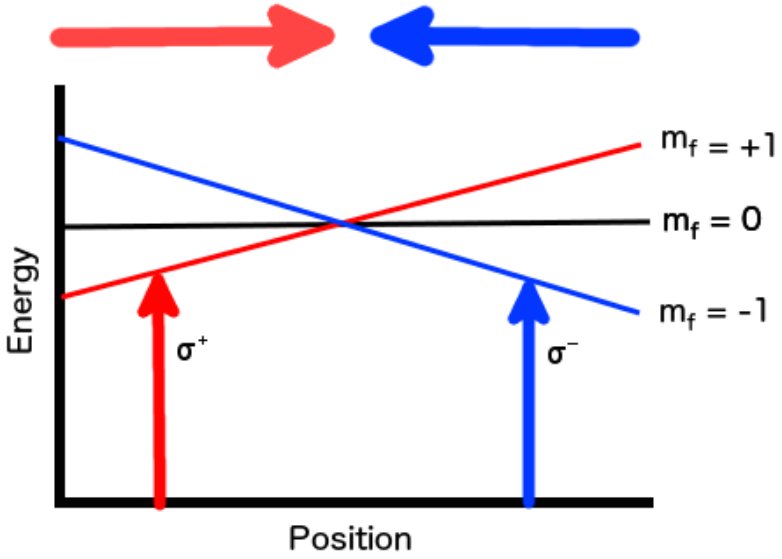


Figure 18: The principle of the MOT where atoms on the left are only resonant with the σ^+ polarised beam coming from the left and atoms to the right with the σ^- polarised beam coming from the right.

In ^{40}K we use the D2 transition to trap the atoms. The hyperfine splitting, which we neglected before, within the $^2P_{3/2}$ manifold is small enough to not influence this transition. However, the hyperfine splitting within the $^2S_{1/2}$ state is approximately 1.2 GHz. Due to off-resonant excitation of atoms in the $F' = 9/2$ can lead to optical pumping into the F = 7/2 ground state. These atoms will not be optically trapped and will fall from the trap due to gravity. To prevent this loss of atoms a repump beam is added which excites atoms from the $^2S_{1/2}$, F = 7/2 to the $^2P_{3/2}$ state manifold, which will pump the atoms back into the laser cooling cycle.

11 2D MOT

A 2D MOT is often used to create a high flux atom beam to load a 3D MOT in an UHV chamber. It provides a convenient way to load the 3D MOT without contaminating the vacuum in the main chamber with hot potassium gas.

In this chapter we first describe the setup used for the 2D MOT (section **??**). Then we will present the results and several improvements that could be made in the future (section **??**). Lastly, we will discuss the new permanent magnets, which are used to create the magnetic field required for the 2D MOT (section **??**).

11.1 Setup

The setup as shown in Figure **??** is used to create the 2D MOT. The 2D MOT requires a 2D quadrupole magnetic field which is created by four permanent magnets. The characteristic parameters of the 2D-MOT beams can be found in Table **??**. The 2D-MOT chamber is heated to 50 °C to reach the required vapour pressure for the 2D MOT to work.

There are two ways to create the counter-propagating beams needed to trap the atoms. One can either use two independent beams or use one beam and retro-reflect it. The advantage of retro-reflecting the beam is that the total amount of power needed for the MOT laser beams is halved. However, one loses the ability to tune the power balance between the two beams as the retro-reflected beam will always be weaker than the incoming beam. For the 2D MOT the advantage of having twice as much power available outweighs the loss of control over the power balance. However, for the 3D MOT it is the other way around.

Property	Value
Detuning trap light	-3Γ
Detuning repump light	-2Γ
Waist trap and repump light	8 mm
Intensity trap light	60 mW
Intensity repump light	20 mW
Magnetic gradient	15 G/cm

Table 6: The parameters used to create the 2D MOT.

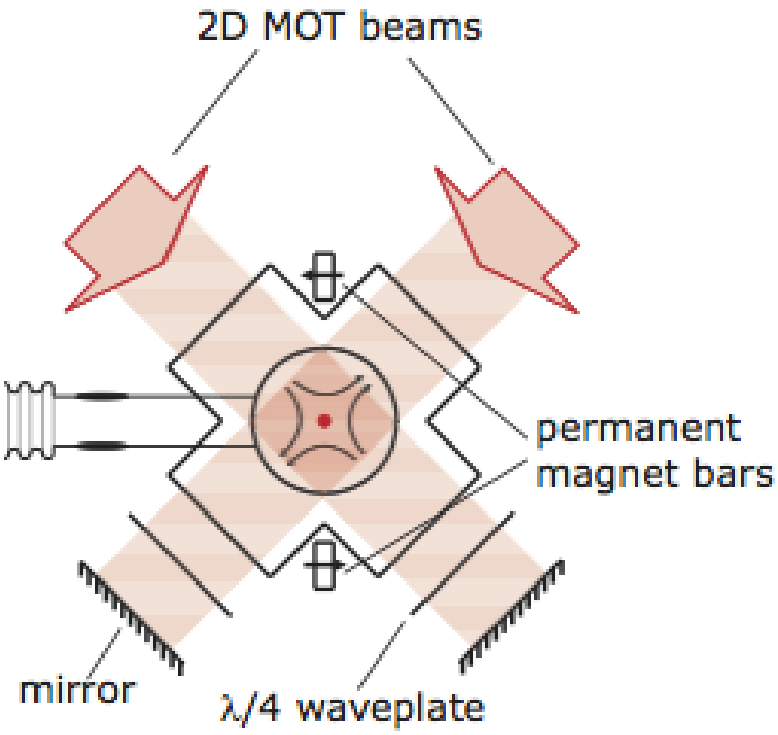


Figure 19: The 3D MOT setup seen along the 2D MOT axes **?**.

11.2 Performance

The 2D MOT currently is able to supply a loading rate of 6×10^6 atoms per second to the 3D MOT. The output flux of the 2D MOT is still significantly lower than previously achieved. This is probably caused by the fact that the waist of the 2D-MOT trap beams currently is half of what it used to be. A straightforward improvement that should be implemented in the future is to increase the waist of the MOT beams as the current laser power is more than sufficient for the current waist. Moreover, the direction of the atomic beam is mostly determined by the alignment of the magnets and the push beam. As the atoms have to go straight through a 2 mm diameter, 23 mm long differential pumping tube the loading rate is very sensitive to this alignment. We have not spend a lot of time on aligning the magnets, so there might be room for improvement here.

11.3 Magnets

The magnets that were originally installed on the machine did occupy space that was needed to place adjustable mirrors and therefore were replaced with smaller magnets. The adjustable mirrors give us precise control over the back reflection of the 2D-MOT

beams. The new magnets have been placed in a smaller mount and are stronger, which allows us to place them further away from the MOT chamber. We used neodymium grade 42 magnets from K&J Magnets. To create a larger width along the magnets with small variations in magnetic field strength two identical magnets are placed in a mount with a spacing of 8 mm. Figure **??** shows the field of the combined magnets measured along the magnets. There still is a relative stable field along 4 cm.

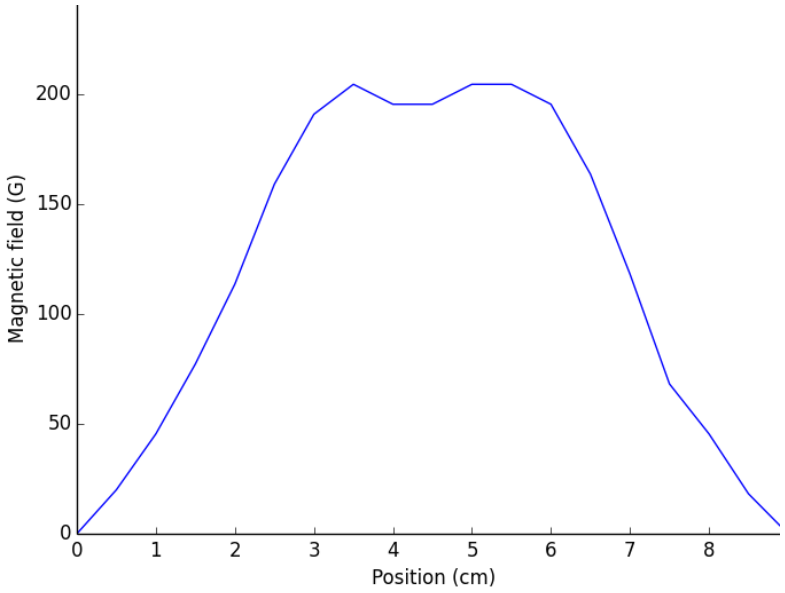


Figure 20: Magnetic field in the radial direction at a distance of 1 cm from the holder.

To determine the magnetic field gradient we build a measurement setup as shown in Figure **??**. We measured the radial component of the magnetic field at two points separated by a distance Δr. The first point is in the middle between the two magnets at zero field. The second point is a centimetre away from the middle in the same direction the beams will follow. From these measurements we calculated the gradient. In this way, we determined the gradient for various distances between the magnets $2R$.

To fit the measured data we have to find the relation between gradient and R. The gradient ∇ is given by $\nabla = C\left(\frac{1}{r^3} - \frac{1}{r'^3}\right)$, where ∇ is the gradient, C is an constant factor and r and r' are shown in Figure **??** . By using the fact that the angle between Δr and R is 45° we can use the cosine rule to express the gradient in terms of Δr and R

$$\nabla = C\frac{2R\Delta r}{(R^2 + \Delta r^2)} = C'\frac{1}{R^3}.$$

For convince we chose Δr to be 1 cm so that the gradient can easily be expressed in Gauss/cm. Using the fit function it is possible to calculate the distance at which the two permanent magnets need to be positioned from the centre of the 2D MOT for a desired magnetic field gradient.

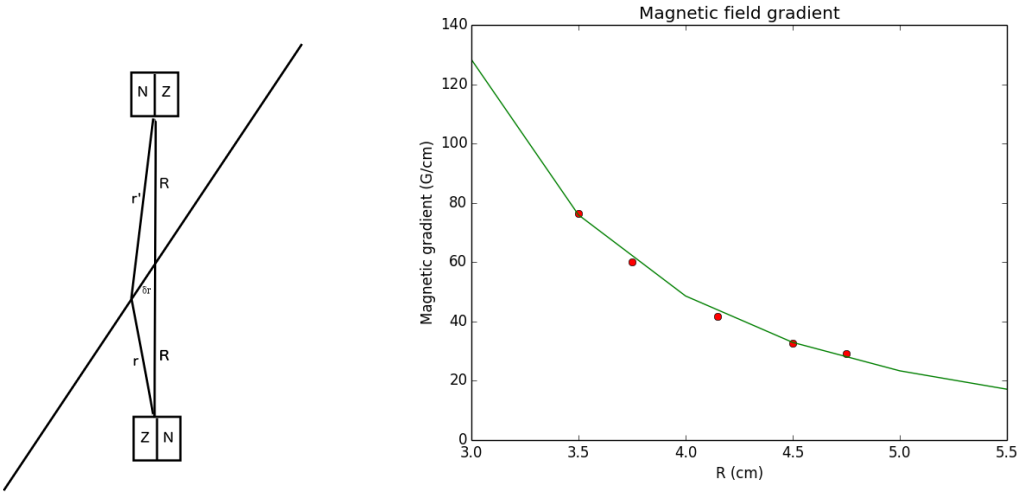


Figure 21: The setup used to determine the magnetic field gradient and the results. Where in the setup the diagonal line shows the direction along which the gradient is measured. R and r give the position vectors used to calculate this gradient.

12 3D MOT

The second step in cooling potassium to a degenerate Fermi gas is the 3D MOT. As the setup has not been used for several years there were some concerns about the quality of the vacuum in the UHV chamber. With measurements of the MOT loading timescale and lifetime we hope to estimate the quality of the vacuum. The determination of the atom number also gives an estimation of the current performance of the setup, which can be compared to measurements taken years ago.

In this chapter we will first discuss the setup used to create a 3D MOT (section **??**). Subsequently, we discuss the fluorescence setup, which is used to determine atom number and lifetime of the MOT (**??**). Lastly, we will discuss our MOT loading and lifetime measurements (section **??**).

12.1 Setup

The 3D MOT uses a six beam configuration, which, compared to the alternative choice of three retro-reflected MOT beams, guarantees a stable MOT beam power balance, independent of the optical density of the MOT. The quadrupole field is created by two electric coils in anti-Helmholtz configuration. The coils are powered by a SM15-200D power supply from Delta Elektronika. The temperature is controlled by water-cooling, a chiller is used to keep the cooling water at 21°C to prevent condensation on both the tubbing and the coils. The coils are used to create a gradient of 14 G/cm in the axial

direction. The experimental parameters used to create the MOT are given in Table **??**. The size of the vertical MOT beams is smaller than the one of the horizontal beams only because the vertical beams are limited in size by the vacuum chamber windows,

Property	Value
Detuning trap light	-3Γ
Detuning repump light	-2Γ
Waist trap and repump light horizontal	11 mm
Waist trap and repump light vertical	7 mm
Intensity trap light horizontal	10 mW
Intensity repump light horizontal	12 mW
Intensity trap light vertical	2.5 mW
Intensity repump light vertical	3 mW
Magnetic gradient	14 G/cm

Table 7: The parameters used to create the 3D MOT.

12.2 Fluorescence imaging

To estimate the atom number and the vacuum lifetime we built a fluorescence imaging setup. The imaging setup consists of biconvex lens with a focal length of 200 mm and a diameter of 50 mm placed 200 mm from the MOT and a photodiode placed 200 mm from the lens. The window of the vacuum system does not clip the light coming from the MOT less than the lens, consequently we can use the full solid angle the lens covers to determine the fraction of photons detected. The solid angle for this setup from which photons are collected is calculated to be 3.9×10^{-3}.

To determine the atom number of the MOT we first need to determine the total number of photons scattered, which depends on the geometry of the setup, the intensity with which the transition is driven and the scattering cross section.

Secondly, to determine the atom number we first need an estimation of how many photons a single atom scatters in all directions. This is determined by two properties: the number of photons and the absorption cross section

$$\sigma = \frac{3\lambda^2}{2\pi} \frac{1}{1 + (2\delta/\Gamma)^2},$$

where $\delta = 3\Gamma$ the detuning of the MOT laser beams from the resonance and $\Gamma = 2\pi \times 6\,\mathrm{MHz}$ is the linewidth of the laser cooling transition **?**. By multiplying the cross section with the number of photons per area we will get the amount of scattered photons, in our case 4×10^6. This results in a total amount of photons scattered by the MOT of 7×10^{13}, if we then divide the total number of scatter photons by the amount of photons a single atom will scatter we can determine the maximum atom number to be 2×10^7.

Compared with previous atom numbers for this setup the atom number is quite low. Previous MOTs had the size of 10^9 atoms. However, due to time constraints we have spend almost no time to optimise the 3D-MOT or the 2D-MOT. Better power matching and spatial overlap between the different MOT beams will most likely improve the 3D MOT.

12.3 Lifetime measurements

To get an estimate of the vacuum quality of the system we determine the loading time and the lifetime of our MOT. To determine the loading time we measure how that atom number increases after the MOT has been destroyed. The atom number is expected to change over time as $\frac{dN(t)}{dt} = \gamma - \beta N(t)$, γ is the loading rate and β is the two-body loss rate coefficient. Solving this differential equation gives $N(t) = \gamma t - \exp(-t/\tau_1)$, where $1/\tau_1$ is the loading time constant.

To determine the MOT lifetime we disable the loading of the 3D-MOT and determine the decay of the MOT in which case we have $\frac{dN(t)}{dt} = -\beta N(t)$, which gives us $N(t) = N_0 - \exp(-t/\tau_2)$, this we call the lifetime of the MOT **?**.

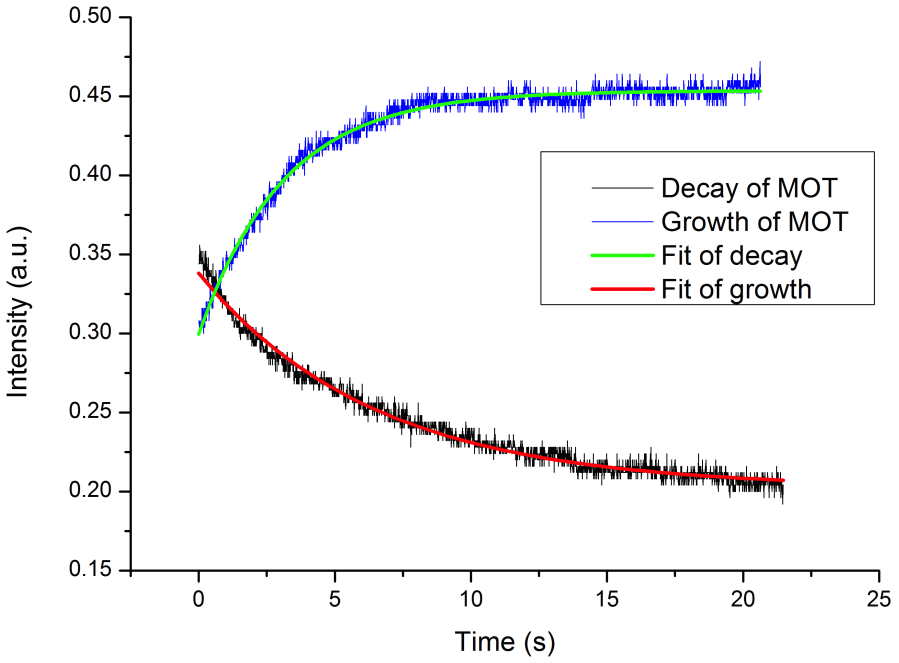


Figure 22: The decay and growth time of the MOT.

We performed these measurements for two cases, with push beam as shown in Figure **??** and without push beam as shown in Figure **??**. The loading time scale and the lifetime are 3.4 seconds and 6.4 seconds, respectively. With push beams they are 2.1 and 4.7 seconds. From the reduction in these values we can conclude that the push beam

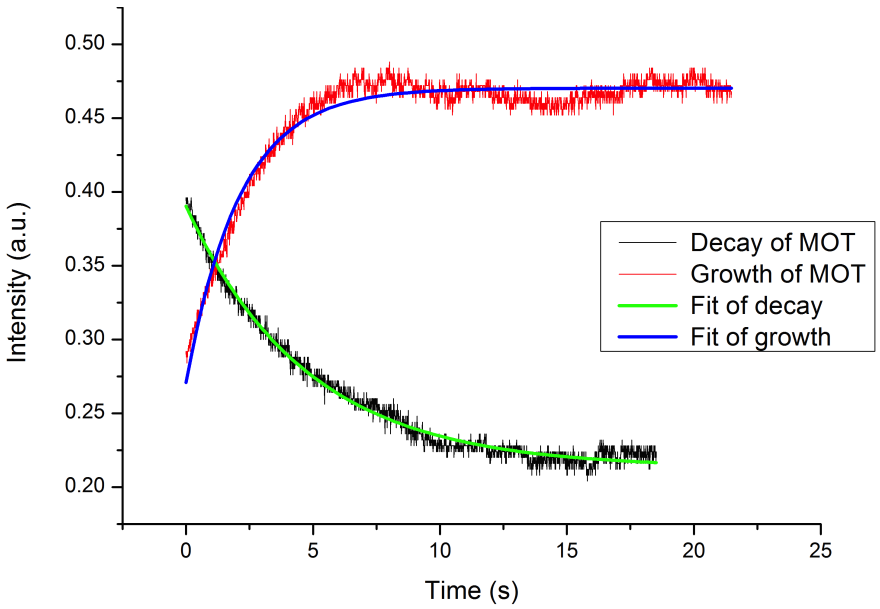


Figure 23: The decay and growth time of the MOT in the presence of the push beam.

has a negative effect on the MOT lifetime and currently has a negligible effect on the loading rate. By properly aligning the magnets and the push beam the loading rate can most likely be increased but currently it is better to operate the machine without push beam.

The lifetimes give good hopes for the vacuum quality. The MOT lifetime is only a lower limit for the vacuum limited lifetime and it already is several seconds, which is enough to for many cold atom experiments.

13 Conclusion

We have been able to successfully build a laser setups needed for a 2D and 3D potassium MOT, which gives us full control over both the power and the detuning of the separate laser beams. The magnets of the 2D MOT have successfully been characterised and replaced.

We have successfully rebuilt the experiment to create a MOT of ^{40}K and measured the lifetime and the loading time of the 3D MOT with and without a push beam. The measured loading time and lifetime is 3.4 seconds and 6.4 seconds. With this we have been able to verify that the vacuum quality inside the machine is sufficient to do most ultra cold atom experiments.

We tried to add a push beam to increase the loading rate of the 3D MOT. However the atom number did not increase significantly while the loading time and lifetime decreased to 2.1 and 4.7 seconds. From this we can conclude that in its current state the push beam is not beneficial.

In the future an absorption imaging setup needs to be constructed to more precisely characterise the MOT and a dipole trap should be installed. After the dipole trap a D1-cooling scheme and evaporative cooling can be utilised to cool the atoms further.

14 Acknowledgements

First of all, I would like to thank Florian for giving me the great opportunity to work on an experiment on my own and trusting me to take care of the potassium lab. Further, I would like to thank him for the extensive and fast corrections he made to this thesis in the last few weeks and lastly for the great parties that he would throw.

Secondly, I would like to thank Benjamin who taught me the difference between doing something fast and doing something well, which will be faster in the end. I'd like to thank him for all the experimental skills he taught me, particularly during the first few months where I learned that after four years of advanced quantum mechanics and many other difficult courses a lot of basic knowledge was still missing. Finally, I would like to thank him for his help especially at the end in getting the 3D MOT to work. Without his help I would never have finished in time.

Thirdly, Maarten for building a functioning laser lock as his bachelors project and thus saving me all the time of doing it. But especially for joining me in a lab that before then sometimes felt a bit lonely.

Namrata for all the help she gave at the end working to achieve the 3D MOT. I also enjoyed our lively discussions about physics, education and the world in general which forced me to think of more decent arguments than: "my intuitions say it should be that way".

Shayne and Chun-Chia for always taking time to answer my questions no matter whether it was high-school material, technical or just difficult. Always having the right tools in a structured place which I could borrow and for letting me join in the lab for the last few weeks where I wrote most of this report to the sound of turbo-pumps. I also would like to note their good taste for chocolate.

I would like to thank Alex for his profound knowledge of electronics and never hesitating to help me with any problems I encountered in the lab.

Both the electronic and mechanical workshops provided invaluable help and expertise when I needed it.

Klaasjan van Druten for being my second supervisor at such a short notice.

Graham, Julius and Nataly for their regular tea breaks to which I would invite myself. I would like to thank Graham for the amount of trust he had in the success of my project, which was extremely motivating.

The rest of the quantum gasses group for all their help and company during the last year.

Lastly, I would like to thank cookies and chocolate for their existence. Without them this project would not have been possible.

References

https://www.rp-photonics.com/external_cavity_diode_lasers.html.

A. S. Arnold, J. S. Wilson, and M. G. Boshier. A simple extended-cavity diode laser. *Review of Scientific Instruments*, 69(3):1236–1239, 1998.

G. Bismut, B. Pasquiou, D. Ciampini, B. Laburthe-Tolra, E. Maréchal, L. Vernac, and O. Gorceix. Optimized loading of an optical dipole trap for the production of chromium becs. *Applied Physics B*, 102(1):1–9, 2011.

C. J. Foot. *Atomic physics*. OUP Oxford, 2004.

G. Lochead. *Excited state spatial distributions in a cold strontium gas*. PhD thesis, Durham University, 2012.

H. Loh, Y.-J. Lin, I. Teper, M. Cetina, J. Simon, J. K. Thompson, and V. Vuletić. Influence of grating parameters on the linewidths of external-cavity diode lasers. *Applied optics*, 45(36):9191–9197, 2006.

A. Ludewig. *Feshbach resonances in* ^{40}K. PhD thesis, 2012.

H. J. Metcalf and P. Van der Straten. *Laser cooling and trapping*. Springer Science & Business Media, 2012.

M. Mooij. Laser lock for laser cooling and trapping of potassium-40. Master's thesis, University of Amsterdam, 2015.

F. Schreck. Control system.

D. A. Smith and I. G. Hughes. The role of hyperfine pumping in multilevel systems exhibiting saturated absorption. *American Journal of Physics*, 72(5):631–637, 2004.

R. J. C. Spreeuw. Quantum optics, lecture notes, 2014.

M. K. M. thesis. Het maken van een diodelasersysteem voor het maken van een magneto-optische val van rubidium-atomen. Master's thesis, University of Amsterdam, 2007.

T. Tiecke. Properties of potassium. *University of Amsterdam, The Netherlands, Thesis*, 2010.

J. Walraven. Atomic physics, 2014.